BIOCHEMISTRY
including biophysical chemistry & molecular biology

Article

pubs.acs.org/biochemistry

High-Resolution Structure of a Protein Spin-Label in a Solvent-Exposed β-Sheet and Comparison with DEER Spectroscopy

Timothy F. Cunningham,[†] Marshall S. McGoff,[†] Ishita Sengupta,[‡] Christopher P. Jaroniec,[‡] W. Seth Horne,*[,†] and Sunil Saxena*[,†]

[†]Department of Chemistry, University of Pittsburgh, 219 Parkman Avenue, Pittsburgh, Pennsylvania 15260, United States

[‡]Department of Chemistry, The Ohio State University, Columbus, Ohio 43210, United States

Supporting Information

ABSTRACT: X-ray crystallography has been a useful tool in the development of site-directed spin labeling by resolving rotamers of the nitroxide spin-label side chain in a variety of α-helical environments. In this work, the crystal structure of a doubly spin-labeled N8C/K28C mutant of the B1 immunoglobulin-binding domain of protein G (GB1) was solved. The double mutant formed a domain-swapped dimer under crystallization conditions. Two rotameric states of the spin-label were resolved at the solvent-exposed α-helical site, at residue 28; these are in good agreement with rotamers previously reported for helical structures. The second site, at residue 8 on an interior β-strand, shows the presence of three distinct solvent-exposed side-chain rotamers. One of these rotamers is rarely observed within crystal structures of R1 sites and suggests that the H_α and S_δ hydrogen bond that is common to α-helical sites is absent at this interior β-strand residue. Variable temperature continuous wave (CW) experiments of the β-strand site showed two distinct components that were correlated to the rotameric states observed in crystallography. Interestingly, the CW data at room temperature could be fit without the use of an order parameter, which is consistent with the lack of the H_α and S_δ interaction. Additionally, double electron electron resonance (DEER) spectroscopy was performed on the GB1 double mutant in its monomeric form and yielded a most probable interspin distance of 25 ± 1 Å. In order to evaluate the accuracy of the measured DEER distance, the rotamers observed in the crystal structure of the domain-swapped GB1 dimer were modeled into a high-resolution structure of the wild type monomeric GB1. The distances generated in the resulting GB1 structural models match the most probable DEER distance within ~2 Å. The results are interesting as they indicate by direct experimental measurement that the rotameric states of R1 found in this crystal provide a very close match to the most probable distance measured by DEER.

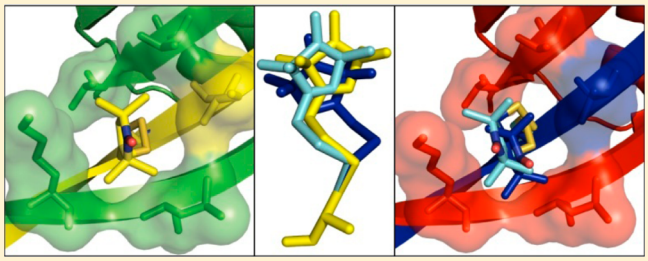

Site-directed spin labeling (SDSL) has emerged as an important biochemical technique that allows application of electron spin resonance (ESR)[1−4] and nuclear magnetic resonance (NMR)[5−7] spectroscopy to explore protein structure and dynamics. A commonly utilized reagent in SDSL is the methanothiosulfonate nitroxide spin label (MTSSL), which reacts with cysteine residues that are introduced via site-directed mutagenesis. The cysteine(s) are reacted with MTSSL to generate the side chain R1 (Figure 1). The continuous wave (CW) ESR line shape of R1 is used to infer information about the identity of protein secondary structure[8] and is often sensitive to the dynamics of the protein backbone.[9,10] However, the deconvolution of spin-label dynamics from protein backbone dynamics typically requires sophisticated analysis.[11−13] SDSL is also essential in the pulsed ESR technique, double electron electron resonance (DEER).[14,15] DEER is used to explore protein structure and conformational changes through the measurement of distance distributions between two spin-labeled sites. However, this experiment does not directly report on the critical distance between the backbone C_α atoms, and thus, a systematic method to derive this distance from the measured interspin distance is needed. In both CW and DEER ESR, complications arise due to the dynamics and/or conformation of the side chain itself. As a result, much work has been done to better understand the conformational preferences of the R1 side chain.

The conformation of the R1 spin label is defined by the five dihedral angles between the protein backbone and the nitroxide ring, denoted χ_1 through χ_5 (Figure 1). The preferred conformations of R1 have been investigated by using X-ray crystallography[16−20] and various computational methods.[21,22] Thus far, the focus has primarily been on spin-label rotamers in surface-exposed α-helical environments. One significant finding from these efforts is the existence of an interaction between H_α and S_δ (Figure 1),[16−20] which is thought to reduce rotational freedom about the first two bonds (χ_1 and χ_2). Since rotation about the disulfide bond (χ_3) is known to be slow, the majority of the R1 mobility has been accredited to rotation about χ_4 and

Received: March 9, 2012
Revised: July 17, 2012
Published: July 18, 2012

   dx.doi.org/10.1021/bi300328w | *Biochemistry* 2012, 51, 6350−6359

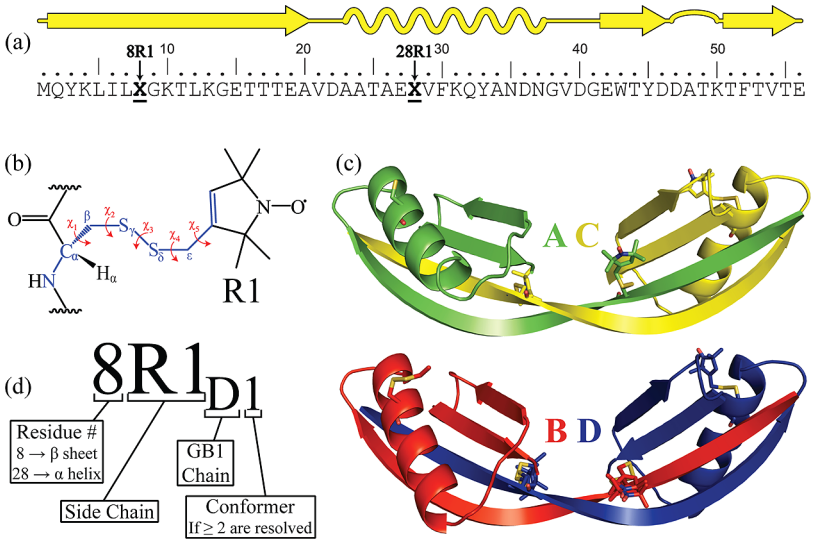

Figure 1. (a) Secondary structure map and sequence of the spin-labeled N8C/K28C GB1 mutant used in this study. The sites labeled with X (8 on a β-sheet and 28 on the α-helix) designate residues mutated to Cys and subsequently labeled with MTSSL. (b) The structure of the R1 residue with side-chain torsions labeled. (c) Two crystallographically independent domain-swapped dimers observed in the crystal structure of the spin-labeled double mutant. Chains A, B, C, and D are colored in green, red, yellow, and blue, respectively. (d) Key for the notation used to identify R1 rotamers is in the text.

χ_5 (this is collectively referred to as the χ_4/χ_5 model[10]). This model is further supported by the rotamers determined by crystallography. In solvent-exposed cases where local interactions are minimal, only χ_1, χ_2, and, occasionally, χ_3 are typically measured, as electron density is not often resolved beyond S_δ, suggesting a higher mobility about χ_4 and χ_5.[16,18,19] Crystal structures of proteins with nitroxide rings containing bulky substituents are also available (PDB IDs 1ZWN and 1ZUR). The χ_4/χ_5 model has been particularly useful in the interpretation of continuous wave (CW) ESR spectra. Given that the χ_4/χ_5 model suggests that the internal motions of the spin label are similar at all surface exposed helical sites, the site-to-site spectral changes in surface exposed helical sites can be directly attributed to fluctuations of the protein backbone, as was shown to be the case with the DNA binding protein, GCN4-58.[23] In cases where R1 is buried, local interactions dominate leading to more restricted motion, and thus, it is common that the entire side chain is fully resolved.[17,20] Since χ_1 and χ_2 are the only consistently measurable angles throughout these studies, the conformation of $\{\chi_1/\chi_2\}$ is commonly presented in the notation m($-60° \pm 20°$), p($+60° \pm 20°$), or t($180° \pm 20°$).[24]

As noted above, the focus of previous R1 conformational studies to date has been on α-helices, including solvent-exposed,[18,19,25] buried,[17] and membrane-embedded sites.[20] In contrast, the spin-label conformations in β-sheet structures have been relatively unexplored. A previous dynamics study by Lietzow et al.[26] investigated R1 in a variety of solvent-exposed β-sheet environments (pleated vs twisted sheet, interior vs edge strand, etc.) using CW ESR. While thorough, many of the important conclusions concerning the $\{\chi_1/\chi_2\}$ conformations used to interpret the ESR results were obtained by in silico modeling rather than by direct crystallographic observation. Additionally, for interior strands, it was concluded that the χ_4/χ_5 model would only hold true if the degree of strand twist was sufficient to sterically allow the H_α and S_δ hydrogen bonding to occur. Recently, the first crystal structure of a protein containing R1 in a β-sheet was published by Freed et al.[27] This work provides a thorough investigation of membrane effects on R1 when located on a membrane-embedded β-barrel. Interestingly, when R1 is present within the lipid environment, the spin label strongly interacts with hydrophobic pockets on the protein surface, which influences the resultant CW spectra. There is, however, no direct structural examination of R1 in solvent-exposed β-sheets, making it difficult to draw direct comparisons with the data set from Lietzow.[26]

The goals of this work are to investigate the conformations of R1 side chains in a solvent-exposed β-sheet, use these results to interpret distance distributions obtained by DEER spectroscopy, and assess the dynamics of R1 located at the β-sheet site using variable temperature CW measurements. To this end, we used the 56-residue B1 immunoglobulin-binding domain of protein G (GB1). GB1 is commonly used as a model system in protein folding studies[28−30] as well as in a variety of other applications[31−34] due to its high stability[35,36] and well understood structure.[35,37−40] The GB1 mutant utilized here includes two spin labels, one on the α-helix and one on the β-sheet (Figure 1a). The crystal structure of this mutant was solved and provided multiple rotameric states of R1 at both locations. DEER spectroscopy was used to measure the interspin distance for the doubly labeled GB1 mutant, allowing for a comparison with the crystal structure. This work provides the initial characterization of R1 rotamers in a solvent-exposed, interior strand, twisted β-sheet. Variable temperature CW analysis of the β-sheet site was also performed to assess the internal motion of R1 at the β-sheet site in light of the resolved rotameric states of R1 at this site. Additionally, a remarkable correspondence between the most probable DEER distance and the predicted distances obtained by modeling the resolved R1 rotamers into a high-resolution WT GB1 structure was observed. This constitutes a promising step toward a general approach for the elucidation of backbone $C_\alpha-C_\alpha$ distances in proteins by DEER spectroscopy.

dx.doi.org/10.1021/bi300328w | *Biochemistry* 2012, 51, 6350−6359

EXPERIMENTAL PROCEDURES

GB1 Expression and Purification. The wild type GB1 plasmid was obtained as a gift from Professor Angela M. Gronenborn (University of Pittsburgh) and used to create a plasmid encoding for the N8C single mutant and the N8C/K28C double mutant by previously described methods.[7] The plasmid was transformed into BL21(DE3) *E. coli* cells, which were subsequently grown in 1 L of LB media with 100 μg/mL of ampicillin. The culture was grown at 37 °C until OD_{600} reached 0.6 to 0.8 at which point IPTG was added to a final concentration of 500 μM. Growth was continued for 4 h, and the cells were pelleted by centrifugation. The pellet was resuspended in 20 mM Tris-HCl at pH 8.5, 5 mM NaCl (buffer A) with 5 mM $MgCl_2$, 1 mM $CaCl_2$, 1 mg/mL lysozyme, 11 units/mL DNase I, 1.3 units/mL RNase A, and 0.1% w/v Triton X-100. The resuspended cells were mixed on ice for 1 h, then sonicated 3 × 30 s. The mixture was centrifuged at 20,000 rpm in a Sorvall SS-34 rotor for 30 min, and the pellet was discarded. The supernatant was placed in an 80 °C water bath for 10 min, then again centrifuged. The supernatant was sterile-filtered (0.22 μm) and loaded onto a GE Healthcare HiTrap Q HP column equilibrated in buffer A. The [NaCl] was increased to 500 mM over 40 mL elution, and individual fractions were checked with SDS−PAGE. The fractions containing GB1 were combined, treated with 10 mM TCEP, concentrated with an Amicon 3,000 MWCO centrifugal filter, and further purified by size exclusion chromatography on a GE Healthcare Sephacryl S-100 26/60 GFC column equilibrated with 150 mM NaCl and 50 mM sodium phosphate at pH 6.5 (buffer B). The GB1 fractions were combined and concentrated to 160 μM (1 mg/mL) with 20% (v/v) glycerol and 10 mM TCEP then flash frozen in liquid nitrogen.

MTSSL Labeling. (1-Oxyl-2,2,5,5-tetramethyl-Δ3-pyrroline-3-methyl) methanethiosulfonate (MTSSL) was purchased from Toronto Research Chemicals. Labeling reactions were performed such that the final MTSSL:GB1 was 20:1. Thus, to label 1 mg (0.16 μmol) of GB1, 0.85 mg (3.2 μmol) of MTSSL was dissolved into 100 μL of DMSO and diluted to 1 mL with buffer B. The N8C/K28C GB1 was thawed and run through a series of 5 × 5 mL GE Healthcare HiTrap desalting columns equilibrated with buffer B to remove TCEP and glycerol. The eluted protein was added directly to the premade MTSSL solution and allowed to react overnight. The mixture was concentrated and again run through the desalting columns to remove excess label. The eluted GB1 was concentrated to 0.25 mM for ESR studies or concentrated to 2.7 mM (17 mg/mL) for crystallographic studies.

Size Exclusion Chromatography. ESR samples were further checked for the possible formation of domain swapped dimers using a GE Healthcare Superdex 75 10/300 GL equilibrated with buffer B. Then, 100 μL of 50 μM spin-labeled N8C/K28C GB1 was injected to the column using a 100 μL loading loop at a flow rate of 0.5 mL/min. The remainder of the 50 μM labeled protein was stored at 4 °C and run under identical conditions for three consecutive days. WT GB1 was run under similar conditions as a basis of comparison.

Crystallization, Data Collection, and Structure Determination. Crystals of the nitroxide-labeled N8C/K28C double mutant of GB1 were grown by hanging drop vapor diffusion. A 17 mg/mL solution of protein in water was mixed (1 μL + 1 μL) with 150 mM sodium acetate at pH 4.5, 18% w/v PEG 3350; the drop was allowed to equilibrate at room temperature over a well containing the crystallization buffer. A single crystal was flash frozen in liquid nitrogen after cryoprotection in well buffer supplemented with 20% v/v glycerol. Diffraction data were collected using CuKα radiation on a Rigaku/MSC diffractometer (FR-E generator, VariMax optics, AFC-Kappa goniometer, Saturn 944 CCD detector) equipped with an X-Stream 2000 low temperature system operated at 100 K. Raw diffraction data were indexed, integrated, and scaled with d*TREK. The crystal diffracted to 2.0 Å resolution with C2 symmetry and unit cell dimensions of a = 105.3, b = 35.8, c = 86.99, β = 126.4°.

Structure solution and refinement were carried out using the CCP4 software suite.[41] The structure was solved by molecular replacement using the program Phaser[42] and a model derived from a published structure of wild type GB1 (PDB ID: 2QMT[43]). Refinement was performed by a combination of Refmac[44] for automated refinement, Coot [45] for manual model building, and ARP/wARP[46] for automated model building. NCS restraints were applied during refinement for all four chains in the asymmetric unit. Geometric restraints for the nitroxide spin label were constructed from a published high-resolution small molecule crystal structure (CSD: 710750).[47] The final model was validated using the MolProbity[48] server and scored in the 87th percentile as compared to 12522 published structures of 2.00 Å ± 0.25 Å resolution. Coordinates and structure factors have been deposited in the Protein Data Bank (PDB ID: 3V3X). Data collection and refinement statistics are listed in Table 1.

Table 1. X-ray Crystal Data Collection and Refinement Statistics for N8R1/K28R1 GB1

data collection	
unit cell dimensions (Å, deg)	a = 105.3, b = 35.8, c = 86.99 $\alpha = \gamma$ = 90; β = 126.4
space group	C2
resolution (Å)	27.3−2.0 (2.07−2.00)
total observations	60,218
unique observations	17,743
redundancy	3.4 (2.7)
completeness (%)	98.8 (94.8)
I/σ	15.5 (3.0)
R_{merge} (%)	4.9 (27.2)
refinement	
resolution (Å)	25.0−2.0
R (%)	23.1
R_{free} (%)	28.8
avg. B factor (Å^2)	36.0
rmsd	
bonds (Å)	0.018
angles (°)	2.2

ESR Measurements and Analysis. All ESR experiments were performed on a Bruker Elexsys 580 spectrometer with a Bruker ER4118X-MD5 resonator. The temperature for all experiments was controlled with an Oxford ITC503 temperature controller and an Oxford ER 4118CF gas flow cryostat.

Approximately 5 μL of spin-labeled GB1 in buffer B and 30% w/v Ficoll 70 was drawn into quartz capillary tubes (1.0 o.d. × 0.8 i.d.) for CW measurements. Spectra were collected at an incident microwave power of 0.1995 mW. The modulation frequency and amplitude were set to 100 kHz and 1 G,

dx.doi.org/10.1021/bi300328w | *Biochemistry* 2012, 51, 6350−6359

Table 2. Spin Label Side Chain Dihedral Angles Resolved for All Rotamers in the N8R1/K28R1 Crystal Structure[a]

mutant	rotamer	χ_1	χ_2	χ_3	χ_4	χ_5	C_α–S dist. (Å)	solvent exposed	structure
$8R1_A$	{m,-120}	−57	−120	−88	−109	61	4.2	no	β-sheet
$8R1_{B1}$	{m,t}	−60	168	85	68	12	3.7	no	
$8R1_{B2}$	{t,p}	−167	74	92	169	102	4.4	no	
$8R1_C$	{m,m}	−56	−74	−76	−93	77	3.6	yes	
$8R1_{D1}$	{m,t}	−59	162	72	61	−94	4.6	yes	
$8R1_{D2}$	{m,m}	−63	−58	−83	−86	74	3.4	yes	
$28R1_A$	{m, - }	−61						no	α-helix
$28R1_B$	{m,m}	−61	−63	112	148		3.5	no	
$28R1_C$	{m,m}	−60	−61	96	140	90	3.3	yes	
$28R1_D$	{m,m}	−58	−66	97	81	−73	3.5	yes	

[a]The C_α–S distance is listed to show which rotamers contain the H_α–S hydrogen bond. The environment of each mutant was individually investigated to assess the validity of referring to each as a solvent-exposed site, and the results are shown in the table.

respectively. Spectra were collected within a temperature range of 293 to 253 K in increments of 10 K. Additionally, a low temperature (80 K) CW spectrum was also collected.

The 80 K CW spectrum was fit using the EasySpin[49] program to find the principal A and g tensor values, which for 8R1 are A_{xx} = 6.4 G, A_{yy} = 5.7 G, and A_{zz} = 37 G, and g_{xx} = 2.0080, g_{yy} = 2.0060, and g_{zz}= 2.0020. The higher temperature spectra were fit with the microscopic order macroscopic disorder (MOMD) model using the NLSL program described by Budil et al.[50] The MOMD model is used to describe the anistropic motion of the R1 side chain with respect to the protein using a series of coordinate frames. The first frame is the magnetic frame of the nitroxide (x_m, y_m, and z_m) where x_m lies along the N–O bond, z_m lies along the p orbital of the N, and y_m completes the right-handed frame. The second frame is the rotational diffusion frame. Spectra were fit assuming an axially symmetric rotational diffusion frame ($R_\parallel$ and $R_\perp$) using the average rotational time $\bar{R} = (R_\parallel R_\perp^2)^{1/3}$ and the asymmetry parameter $N = R_\parallel/R_\perp$. The rotational correlation time of R1 (τ) is equal to $1/6\bar{R}$. Transformation between the magnetic frame and the rotational frame is defined by three Euler angles, α_D, β_D, and γ_D. Fitting of the spectra here, as seen previously, was found to depend primarily on angle β_D. Over the specified range of temperatures, β_D was assumed to remain constant. Previous work with solvent-exposed α-helices[10,23] and β-sheets[26] has shown that holding β_D at 36° provided sufficient fits; however, for the 8R1 spectra presented here, higher quality fits resulted when β_D was held at 32°. Additionally, the MOMD model includes an ordering potential that is commonly utilized to fit spectra of R1 at solvent-exposed α-helical sites; however, an order parameter, S_{20} was not required for fits of the experimental spectra. Therefore, only $\bar{R}$, N, and the Gaussian inhomogeneous line width, gib0, were varied for all fits with the priority of fitting the width of the central line and the low field peak.

For the DEER experiment, the pulse sequence used was $(\pi/2)\nu_1$-τ_1-$(\pi)\nu_1$-T-$(\pi)\nu_2$-τ_2-$(\pi)\nu_1$-τ_2-echo.[15] The pump frequency (ν_2) was placed at the maximum of the nitroxide spectrum, and the observer frequency (ν_1) was offset ∼67 MHz at the maximum of the low field component. The length of the $(\pi/2)\nu_1$ and $(\pi)\nu_1$ pulses were set to 16 and 32 ns, respectively, while the $(\pi)\nu_2$ pulse was set to 16 ns. The parameters τ_1 and T were set to 200 and 160 ns, respectively, and T was incremented by a stepsize of 10 ns for 256 points; τ_2 was adjusted such that $T + \tau_2$ = 2760 ns. The raw time domain DEER spectrum was analyzed using DEER Analysis 2008.[51]

RESULTS

Design of the Double Mutant. Crystallographic structure determination and ESR experiments were performed on an MTSSL spin-labeled N8C/K28C GB1 mutant. The K28 site in the WT protein resides on an α-helix which allowed us to compare our results with the literature. The N8 site is located on the β-sheet and serves to provide new insight into R1 rotamers on solvent-exposed β-sheets. The double mutant enables the use of DEER spectroscopy to acquire distance constraints that are compared with the crystallographic results.

N8R1/K28R1 GB1 Crystal Structure. The spin-labeled N8C/K28C GB1 double mutant crystallized as a domain-swapped dimer Figure 1c, which was refined to 2.0 Å (Table 1). The asymmetric unit comprises two dimers for a total of four crystallographically independent GB1 chains. The four different monomers are labeled A, B, C, and D (shown in green, red, yellow, and blue, respectively), and the dimers are paired A/C and B/D. Each of the four GB1 monomers has two R1 residues (Figure 1), one at site 8R1 on the β-sheet and the other at site 28R1 on the α-helix. For some R1 residues, two different partial-occupancy rotamers were visible in electron density. The notation utilized to differentiate between the various R1 rotamers in the asymmetric unit is illustrated in Figure 1d.

Spin-Label Rotamers. All R1 rotamers are defined by the five dihedral angles, χ_1 through χ_5 (Figure 1b). In total, there are six β-sheet (8R1) and four α-helix (28R1) rotamers which were at least partially resolved in the crystal structure. The values of the dihedral angles χ_1 through χ_5 for all rotamers are displayed in Table 2. As a means of comparison with previous work,[18,26] the $\{\chi_1,\chi_2\}$ conformation for all rotamers are also presented in Table 2 in the m, p, and t notation (−60° ± 20°, +60° ± 20°, and 180° ± 20°, respectively).[24]

At the four 28R1 α-helical sites in the asymmetric unit, only two of the four side chains, $28R1_C$ and $28R1_D$, are fully resolved. In this nomenclature, C and D refer to the GB1 chain on which the rotamer is located. Both rotamers have $\{\chi_1,\chi_2\}$ conformations of {m,m} type. The C_α to S_δ distances for $28R1_C$ and $28R1_D$ are 3.3 Å and 3.5 Å, respectively. These distances suggest the possible presence of a C_α—$H_\alpha\cdots S_\delta$ hydrogen bond.[19] The {m,m} conformation and the presence of this hydrogen bond have been reported previously for rotamers located within a solvent exposed, α-helix environment.[18] Thus, our results are reasonable given the location of 28R1 within GB1. In addition, the disulfide dihedral angle (χ_3) for both $28R1_C$ and $28R1_D$ is ∼+90°. This agrees with previous computational results that χ_3 of either +90° or −90° are commonly populated.[21,22] Previously published R1 residues in a

dx.doi.org/10.1021/bi300328w | Biochemistry 2012, 51, 6350–6359

solvent-exposed α-helix with a $\{\chi_1,\chi_2\}$ conformation of {**m,m**} show a value of −90° for χ_3.[18]

Four unique 8R1 sites exist within the crystal asymmetric unit, and two of these sites (on chains B and D) contain two distinct partially occupied R1 rotamers. Therefore, there are a total of six different β-sheet rotamers (Table 2). In order to determine which positions were good models for a solvent-exposed β-sheet, the environment of each site was individually examined. The $8R1_A$ and $8R1_B$ side chains appear to be perturbed by local contacts. For $8R1_A$ (Figure 2a), residue

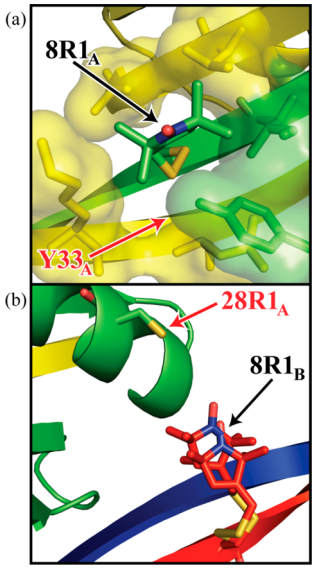

Figure 2. Local environments for $8R1_A$, $8R1_{B1}$, and $8R1_{B2}$. (a) For $8R1_A$, residue $Y33_A$ from a crystallographic symmetry mate is located within 3.5 Å of the nitroxide and is likely perturbing this rotamer. (b) For $8R1_B$, the $28R1_A$ rotamer is pointing directly into the same physical space as both $8R1_B$ rotamers. Although $28R1_A$ is not fully resolved, the 5.1 Å distance between the $28R1_A$ S_γ and $8R1_B$ makes it highly likely that the movement/conformation of both sites are influenced by each other.

$Y33_A$, from a symmetry copy of chain A is in close proximity to the nitroxide (~3.5 Å). At site $8R1_B$, two resolved R1 rotamers were observed ($8R1_{B1}$ and $8R1_{B2}$ in Figure 2b). Both $8R1_B$ rotamers point into the same physical space as the $28R1_A$ rotamer. Although $28R1_A$ is not fully resolved, it is likely that $28R1_A$ and $8R1_B$ are interacting with each other especially given the proximity of the S_γ from $28R1_A$ to both of the $8R1_B$ rotamers (~5.1 Å). For these reasons, $8R1_A$, $8R1_{B1}$, and $8R1_{B2}$ were considered to be perturbed by the non-native environment surrounding each site and thus excluded from further analysis.

The environments for $8R1_C$, $8R1_{D1}$, and $8R1_{D2}$ show no local contacts arising from crystal lattice artifacts and can therefore be characterized as solvent exposed. Residues from chains A and C form an open pocket around $8R1_C$ (Figure 3a). A similar pocket formed by the residues from chains B and D is observed for the rotamers $8R1_{D1}$ and $8R1_{D2}$ (Figure 3b). The environments of these rotamers can be further categorized as an interior strand on a twisted sheet (Figures 3a and b). The $\{\chi_1,\chi_2\}$ conformations of these three solvent-exposed, interior strand, twisted β-sheet rotamers are {**m,m**} ($8R1_C$ and $8R1_{D2}$) and {**m,t**} ($8R1_{D1}$) (see Table 2), and an overlay of all three rotamers is shown Figure 3c.

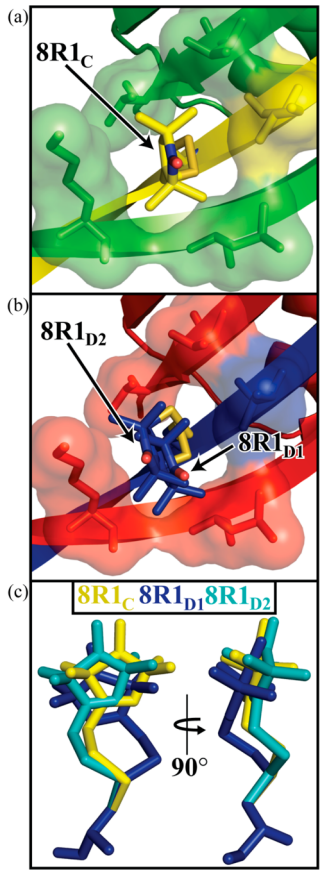

Figure 3. Local environments for (a) $8R1_C$, (b) $8R1_{D1}$, and $8R1_{D2}$. All three rotamers shown above are undisturbed by any protein contacts arising from the crystal lattice. (c) An overlay of the three 8R1 rotamers from a and b.

N8R1/K28R1 GB1 DEER Data and Comparison with Crystal Structure. DEER spectroscopy was performed to examine the interspin distance in the context of side chain packing trends. DEER resolves the interspin distance distribution between two spin-labeled sites. However, it is important to know whether the DEER results are obtained from dimerized GB1 (as in the crystal) or GB1 monomers.

In the crystal, the doubly labeled GB1 mutant formed a domain swapped dimer, but this is not the native structure of wild-type protein. This is not unexpected since certain GB1 mutants have shown a propensity for the formation of domain-swapped dimers; however, the specific mechanism here (interchange of the N-terminal strands between two chains) has not been previously observed for GB1.[52,53] The closest literature precedent for the fold we observed is swapping of the C-terminal β-strand in the B1 domain of protein L.[54,55] Figure 4a shows the structure of a single WT GB1 molecule, as determined by solid-state NMR (PDB ID: 2LGI[40]), and Figure 4c shows the domain-swapped dimer structure presented here. Figure 4b shows the structure of a single GB1 chain within this specific domain swapped dimer. The first strand of the β-sheet (upon which 8R1 is located) is swapped with the same domain from the second GB1 monomer resulting in this specific domain-swapped dimer structure. Size exclusion chromatography was used to investigate the oligomeric state of GB1 in solution under buffer conditions used for the DEER measurements. After three days in the same buffer conditions as the DEER measurements, the elution volume for the mutant was

dx.doi.org/10.1021/bi300328w | *Biochemistry* 2012, 51, 6350−6359

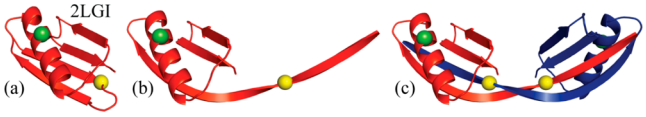

Figure 4. Domain swapping observed in the crystal structure of the N8R1/K28R1 GB1 double mutant. (a) The native monomer fold of GB1 (PDB: 2LGI); the two labeled sites are shown in yellow (N8R1 on the β-sheet) and green (K28R1 on the α-helix). Exchange of the N-terminal β-strand between two chains (b) results in the domain-swapped dimer observed in the crystal structure (c).

consistent with that of the GB1 monomer (see Supporting Information), indicating that the formation of the domain-swapped dimer is a result of the specific crystallization conditions employed in this study.

The results of the DEER experiment are shown in Figure 5. The main panel shows the baseline subtracted time domain

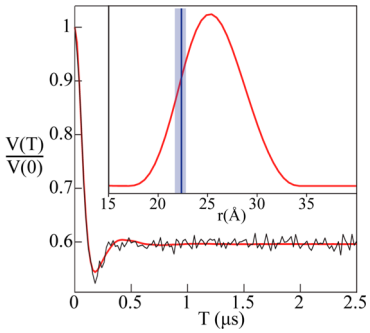

Figure 5. Baseline subtracted time-domain DEER data from the N8R1/K28R1 GB1 sample (black) with the best fit from *DEER Analysis 2008* (red). The inset figure is the resulting distance distribution (red) with an average distance of 26 Å and a most probable distance of 25 Å (suggesting a naturally folded GB1 sample). As a means of comparison between this distribution and the resolved rotamers, the 8R1 and 28R1 rotamers were modeled into a NMR WT GB1 structure (PDB ID: 2LGI shown in Figure 4a) at the appropriate locations. The vertical line (blue) represents the average nitroxide N–N distance between the 8R1 β-sheet rotamers and the 28R1 α-helix rotamers (22.4 Å), and the light blue area is the full range of generated distances.

data (black) with the best fit from DEER Analysis 2008[51] (red). The inlay in Figure 5 shows the resulting distance distribution (red). These results further support the existence of only monomers and no dimers within the ESR sample. If dimers were present, multiple distances would be observed (as there would be four different labels within close proximity) but in this case, only one is observed. Also, the modulation depth of the time domain signal is consistent with only two spins per species (see Supporting Information) which is expected for one doubly labeled GB1 monomer.[56] DEER was also performed on the doubly labeled GB1 mutant in the crystal buffer conditions (150 mM sodium acetate at pH 4.5, 18% w/v PEG 3350) as a means to further investigate the formation of the dimer. The result (data not shown) is very similar to the data shown in Figure 5, and thus, the buffer does not appear to induce dimerization at low protein concentration.

The distance distribution between the two spin labels in the monomeric GB1 shows a most probable distance of 25 Å. In the high-resolution structure of monomeric WT GB1 (PDB ID: 2LGI), the N8 C_α to K28 C_α distance is 18 Å.[40] Given this distance and the approximate length of the R1 chain, a 25 Å interspin is reasonable for monomeric GB1. The DEER data were also compared to the modeling program by Polyhach and Jeschke,[57] and the model predicts the same most probable distance of 25 Å, but the overall distribution was narrower.

8R1 Variable Temperature CW ESR. As a means to explore the dynamics that coincide with rotamers described above for 8R1, variable temperature CW spectra were collected for the 8R1 single mutant. Buffer conditions for the single mutant were identical to that of the DEER sample (buffer B) except for the addition of 30% w/v Ficoll 70. With 30% w/v Ficoll 70, the rotational correlation time of global tumbling of GB1 (≈80 ns) does not substantially contribute to the CW ESR spectral lineshapes.[23] The spectra were collected over the range of 253 to 293 K in increments of 10 K. The resultant spectra with best fits from the MOMD model are shown in Figure 6, and the parameters for the best fits are listed in Table 3.

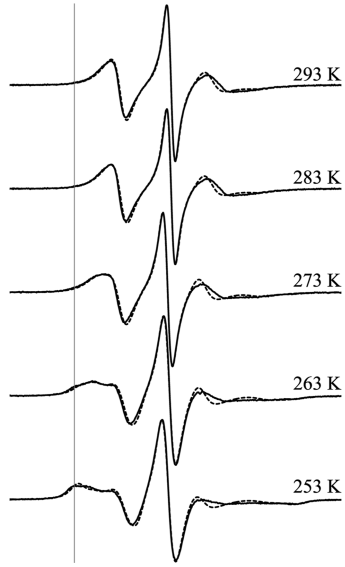

Figure 6. Variable temperature CW spectra for the N8R1 single mutant in buffer B with 30% w/v Ficoll 70 (solid) and the fits (dotted) using the MOMD model. For all spectra, β_D was held constant at 32°. For the spectra at 263 and 253 K, a second component was necessary for fitting, and the vertical gray line is a guide for visualizing the second component. All simulations shown in the figure are with S_{20} = 0. Adequate fits to the second component could, however, be achieved using a range of order parameters (see text).

At temperatures between 293–273, the 8R1 CW spectra contain only a single highly mobile component. An additional

Table 3. Parameters Used to Simulate the N8R1 Single Mutant CW Spectra[a]

temperature (K)	N	τ (ns)	S_{20}	occupancy (%)
293	25	2.1	0	100
283	25	2.2	0	100
273	25	2.9	0	100
263 comp 1	25	4.1	0	81
263 comp 2	20	14.2	0	19
253 comp 1	25	4.6	0	62
253 comp 2	20	19.6	0	38

[a]The fits are shown in Figure 6. Note that a range of order parameters could be used for the second component (see text).

dx.doi.org/10.1021/bi300328w | *Biochemistry* 2012, 51, 6350–6359

component, which exhibits lower mobility, is observed at lower temperatures. At 293 K, the spectrum could be fit with a rotational correlation time, τ, of 2.1 ns, and an order parameter, S_{20}, of 0. The order parameter and rotational correlation times are, however, correlated, and we could obtain similar quality fits with τ in the range of 2.0−2.1 ns by adjusting S_{20} in the range of 0−0.11. These parameters are indicative of highly mobile (low τ) and, at best, a very weakly ordered motional behavior for R1 at this site. The spectra collected at 263 and 253 K contained two components. The main component was consistent with the motion described above with $\tau \approx 4.1$ and 4.6 ns, respectively. At these values of τ, the order parameter was 0. However, a second component, with a much slower rotational rate, was necessary for a quality fit. Given the low population of this component (∼15−19% at 263 K), the spectral features could be simulated with a range of correlation times and order parameters for the second component. At 263 K, for example, we could obtain similar quality fits with τ in the range of 13.2−21 ns by adjusting S_{20} in the range of 0−0.7 as well as the relative populations of the two components.

DISCUSSION

The goal of this study was to resolve the R1 side chain in both an α-helix and β-sheet using X-ray crystallography and to compare these results with distances determined by DEER spectroscopy. Additionally, the β-sheet site was further investigated using variable temperature CW to assess the dynamics of R1 at this site. The first goal was accomplished by spin labeling the N8C/K28C double mutant of GB1 and solving the crystal structure. The structure that resulted was a domain-swapped dimer. While this result was unexpected, it offers multiple advantages. First, we were able to obtain twice as many resolved R1 residues as compared to the natively folded GB1 structure. In addition, the asymmetric unit of this crystal provided two dimers and therefore a total of four different GB1 chains with resolved R1 residues. This greatly increased the probability of finding fully resolved residues that were not perturbed by crystal lattice contacts, which in this case led to two α-helix rotamers ($28R1_C$ and $28R1_D$) and three β-sheet rotamers ($8R1_C$, $8R1_{D1}$, and $8R1_{D2}$). The α-helix rotamers allow the direct comparison with literature, and the β-sheet rotamers offer new insight into the spin-label conformations in a β-sheet context. An additional advantage that came about with the dimer was the β-sheet environment where 8R1 is located. In monomeric GB1 (Figure 4a), the 8R1 site (yellow) lies very close to a β-turn. Within the dimer (Figures 1a and 4b and c), the 8R1 site is located in the middle of a lengthy β-sheet, far away from any turns. This removes the possibility that the 8R1 rotamers are biased by the proximity to a β-turn.

The β-sheet (8R1) rotamers found here are categorized as solvent-exposed rotamers on an interior strand of a twisted β-sheet and have either an {**m,m**} ($8R1_C$ and $8R1_{D2}$) or an {**m,t**} ($8R1_{D1}$) $\{\chi_1,\chi_2\}$ conformation. An assessment of the environment is important due to the previous dynamics study by Lietzow et al. in which a similar environment was investigated on cellular retinol binding protein (CRBP) using CW ESR methods.[26] Using the ESR data as a starting point, they modeled the R1 side chain into the respective locations on the WT CRBP crystal structure. They predicted that in the solvent-exposed, interior strand, twisted sheet environment, the two most likely conformations for R1 would be {**m,m**} and {**m,t**}. The unperturbed 8R1 rotamers presented here match these predictions. Another interesting correlation with Lietzow's work is the $H_\alpha-S_\delta$ hydrogen bond that is probable for many of the rotamers. For both {**m,m**} 8R1 rotamers, this bond is likely present (as indicated by the relatively short $C_\alpha-S_\delta$ distance in Table 2), while in the {**m,t**} rotamer, the $C_\alpha-S_\delta$ distance is too long and precludes the existence of a $H_\alpha-S_\delta$ hydrogen bond. This trend matches well with Lietzow's observations in that {**m,m**} conformations are able to form this hydrogen bond leading to more restrained movement. However, {**m,t**} conformations are unable to form this hydrogen bond and are therefore more mobile.[26]

The rotamers $8R1_C$, $8R1_{D1}$, and $8R1_{D2}$ were found to be viable solvent-exposed, interior strand, twisted β-sheet rotamers. This work is important due to the general lack of X-ray crystallography-based, β-sheet R1 rotameric studies. The recent study by Freed et al.[27] thoroughly investigated β-sheet rotameric states of R1 within membranes. The membrane-embedded environment of Freed's study differs from the solvent-exposed environment investigated here. Such differences in environment are important given that the $\{\chi_1,\chi_2\}$ conformations of the rotamers found in that study are different ({**t,m**} and {**p,p**} vs {**m,m**} and {**m,t**}).

While the rotameric states of R1 observed in this crystal structure provide new structural information for R1 located on a solvent-exposed β-sheet, the variable temperature CW spectra of 8R1 allow analysis of the R1 side chain dynamics at this site. The spectra that are observed over the measured temperature range show a main component of very fast, non or weakly ordered motion with a second less mobile component becoming more obvious at temperatures of the 263 and 253 K regime (Figure 6).

At solvent-exposed sites on α-helices, an order parameter, S_{20}, is commonly needed to fit the spectra in the context of the MOMD model.[10,19,23] The order parameter reflects the restriction in amplitude of the spin-label motion due to the backbone. The need for S_{20} is commonly attributed to the ordering that results from the $H_\alpha-S_\delta$ interaction as described by the χ_4/χ_5 model. Therefore, for solvent-exposed α-helical sites where the internal motion of R1 is well understood, decreased order is interpreted as an increase in backbone fluctuations. In the higher temperature spectra for 8R1 in GB1, S_{20} is not necessary for quality fits using the MOMD model. For the 8R1 site, the relatively low crystallographic *B*-factor of C_α suggests very limited fluctuation of the backbone. Therefore, the most likely cause for the lack of order is that the $H_\alpha-S_\delta$ hydrogen bond is not present at this site. Thus, this component is likely due to the {**m,t**} rotamer observed in the crystal structure for $8R1_{D1}$ in which R1 is geometrically unable to form the $H_\alpha-S_\delta$ interaction. At decreased temperatures, the appearance of a less mobile component suggests a weak interaction that restricts the motion of R1. The spectral features from this component were weakly sensitive to order parameters. Since {**m,m**} is the only other rotamer found at the 8R1 site within the crystal, this weak interaction may be the formation of the $H_\alpha-S_\delta$ hydrogen bond that is present in the {**m,m**} rotameric state. The CW results suggests that the {**m,t**} conformer is dominant at room temperature, which indicates that the interpretation of order parameters in terms of backbone fluctuations should be undertaken with caution in the case of β-sheets, a point that was also made recently by Freed et al.[27]

DEER ESR was performed on the doubly spin-labeled GB1 mutant. DEER spectroscopy is able to resolve distance distributions between two spin-labeled sites. While this

dx.doi.org/10.1021/bi300328w | *Biochemistry* 2012, 51, 6350−6359

technique has been advantageously utilized in many previous studies, the added distance of the spin-label side-chain has been a source of complication as the experiment does not directly report on the $C_\alpha-C_\alpha$ distance. Here, DEER was performed on the doubly labeled N8C/K28C GB1 mutant in order to compare the resulting distance distribution with distances predicted in the crystal structure. The DEER results were obtained on GB1 in its monomeric form and therefore are not directly comparable to the crystal structure. However, this domain-swapping allowed the opportunity to apply the rotamers to a related system with very similar spin-label environments and compare the distances between rotamers with the DEER distribution. This was accomplished by modeling in the R1 side chain into the high resolution WT GB1 structure (PDB ID: 2LGI) at sites N8 and K28, then adjusting all the R1 dihedral angles (χ_1 through χ_5) to match the conformations of the R1 side chains found within the crystal structure.

The distance distribution obtained by DEER is compared to the distances obtained by modeling the rotamers in the inlay of Figure 5. The three 8R1 and two 28R1 rotamers were modeled at the respective locations within WT GB1, and nitroxide N to nitroxide N distances were generated. The light blue area in Figure 5 represents the full range of generated distances (21.7 Å to 22.8 Å), and the solid blue line represents the average distance (22.4 Å). These distances are ∼2−3 Å shorter than the most probable DEER distance of 25 Å. The results are encouraging given that the error in the most probable distance is approximately ±1 Å. The slight difference between the DEER and modeling results can possibly be due to minor changes in R1 rotamer packing that may occur upon crystallization or due to the presence of glycerol in the DEER experiments. Interestingly, when the χ_3 value for the α-helix (28R1) rotamers is altered from the +90° orientation observed in the crystal to the other common χ_3 orientation of −90°,[18,21,22] the mean distance between rotamers increases to 25.5 Å, a distance that closely matches the most probable distance from the DEER distribution. The results are interesting as they indicate by direct experimental measurement that the rotameric states of R1 found in this crystal provide a very close match to the most probable distance measured by DEER. These results foreshadow future work that explores the full conformational preferences of the spin label in solvent accessible β-sheets by modeling. An understanding of the range of orientations of the spin label can lead to methods by which DEER distributions are analyzed to extract constraints on $C_\alpha-C_\alpha$ distance distributions. One such approach was presented recently by Sarver et al.[58] In this work, a series of DEER measurements between multiple sites on a protein−DNA complex were coupled with molecular dynamics (MD) simulations of R1 at the labeled sites. This combination of techniques was able to report directly on the $C_\alpha-C_\alpha$ distribution between the labeled sites.

This distance comparison performed in this work demonstrates the utility of coupling X-ray crystallography resolved rotamers with DEER spectroscopy. Simply modeling resolved rotamers of similar environment (solvent accessibility, secondary structure, etc.) into appropriate locations within a wild type monomer structure resulted in the generation of a mean distance within ∼2 Å of the most probable DEER distance. In other words, this combination of techniques could possibly be used to elucidate the $C_\alpha-C_\alpha$ distance simply from the most probable distance between two labeled sites and an appropriate selection of rotamers. In addition to the characterization of R1 motional modes using X-ray crystallography and variable temperature CW, these results provide important first steps toward a greater understanding of R1 side-chain packing trends in solvent-exposed β-sheets.

■ ASSOCIATED CONTENT

Supporting Information

Size exclusion chromatograms, DEER modulation depth results, and stereo views of electron density around nitroxide modified residues. This material is available free of charge via the Internet at http://pubs.acs.org.

Accession Codes

Coordinates and structure factors have been deposited with the Protein Data Bank: 3V3X.

■ AUTHOR INFORMATION

Corresponding Author

*Phone: (412) 624-8680. Fax: (412) 624-8611. E-mail: horne@pitt.edu (W.S.H.); sksaxena@pitt.edu (S.S.).

Funding

This work was supported by the National Science Foundation (MCB 1157712 grant) to S.S. and the University of Pittsburgh (W.S.H.). The protein mutation work was supported by the National Science Foundation CAREER Award (MCB 0745754) to CPJ.

Notes

The authors declare no competing financial interest.

■ ACKNOWLEDGMENTS

We thank Professor Angela M. Gronenborn (Department of Structural Biology, University of Pittsburgh) for her generous gift of wild type GB1 plasmid. We thank Professor Michael Trakselis (Department of Chemistry, University of Pittsburgh) for use of his facilities for purifying GB1, as well as his lab member, Robert Bauer, for helpful discussions. We thank Jessica Sarver for her helpful comments on the manuscript.

■ ABBREVIATIONS USED

SDSL, site-directed spin labeling; ESR, electron spin resonance spectroscopy; NMR, nuclear magnetic resonance spectroscopy; MTSSL, methanothiosulfonate spin label; R1, resulting side chain from the reaction of MTSSL with free cysteine; CW, continuous wave; DEER, double electron electron resonance; GB1, B1 immunoglobulin-binding domain of protein G; WT, wild type; IPTG, isopropyl β-D-1-thiogalactopyranoside; TCEP, tris(2-carboxyethyl)phosphine; DMSO, dimethyl sulfoxide; MD, molecular dynamics

■ REFERENCES

(1) Hubbell, W. L., and Altenbach, C. (1994) Investigation of structure and dynamics in membrane proteins using site-directed spin labeling. *Curr. Opin. Struct. Biol. 4*, 566−573.

(2) Hubbell, W. L., Gross, A., Langen, R., and Lietzow, M. A. (1998) Recent advances in site-directed spin labeling of proteins. *Curr. Opin. Struct. Biol. 8*, 649−656.

(3) Hubbell, W. L., Cafiso, D. S., and Altenbach, C. (2000) Identifying conformational changes with site-directed spin labeling. *Nat. Struct. Biol. 7*, 735−739.

(4) Columbus, L., and Hubbell, W. L. (2002) A new spin on protein dynamics. *Trends Biochem. Sci. 27*, 288−295.

(5) Battiste, J. L., and Wagner, G. (2000) Utilization of site-directed spin labeling and high-resolution heteronuclear nuclear magnetic

resonance for global fold determination of large proteins with limited nuclear overhauser effect data. *Biochemistry 39*, 5355−5365.
(6) Liang, B., Bushweller, J. H., and Tamm, L. K. (2006) Site-directed parallel spin-labeling and paramagnetic relaxation enhancement in structure determination of membrane proteins by solution NMR spectroscopy. *J. Am. Chem. Soc. 128*, 4389−4397.
(7) Nadaud, P. S., Helmus, J. J., Hofer, N., and Jaroniec, C. P. (2007) Long-range structural restraints in spin-labeled proteins probed by solid-state nuclear magnetic resonance spectroscopy. *J. Am. Chem. Soc. 129*, 7502−7503.
(8) Mchaourab, H. S., Lietzow, M. A., Hideg, K., and Hubbell, W. L. (1996) Motion of spin-labeled side chains in T4 lysozyme. Correlation with protein structure and dynamics. *Biochemistry 35*, 7692−7704.
(9) Mchaourab, H. S., Oh, K. J., Fang, C. J., and Hubbell, W. L. (1997) Conformation of T4 lysozyme in solution. Hinge-bending motion and the substrate-induced conformational transition studied by site-directed spin labeling. *Biochemistry 36*, 307−316.
(10) Columbus, L., Kalai, T., Jeko, J., Hideg, K., and Hubbell, W. L. (2001) Molecular motion of spin labeled side chains in alpha-helices: analysis by variation of side chain structure. *Biochemistry 40*, 3828−3846.
(11) Barnes, J. P., Liang, Z., McHaourab, H. S., Freed, J. H., and Hubbell, W. L. (1999) A multifrequency electron spin resonance study of T4 lysozyme dynamics. *Biophys. J. 76*, 3298−3306.
(12) Liang, Z., Lou, Y., Freed, J. H., Columbus, L., and Hubbell, W. L. (2004) A multifrequency electron spin resonance study of T4 lysozyme dynamics using the slowly relaxing local structure model. *J. Phys. Chem. B 108*, 17649−17659.
(13) Zhang, Z., Fleissner, M. R., Tipikin, D. S., Liang, Z., Moscicki, J. K., Earle, K. A., Hubbell, W. L., and Freed, J. H. (2010) Multifrequency electron spin resonance study of the dynamics of spin labeled T4 lysozyme. *J. Phys. Chem. B 114*, 5503−5521.
(14) Milov, A. D., Ponomarev, A. B., and Tsvetkov, Y. D. (1984) Electron-electron double resonance in electron spin echo: model biradical systems and the sensitized photolysis of declain. *Chem. Phys. Lett. 110*, 67−72.
(15) Martin, R. E., Pannier, M., Diederich, F., Gramlich, V., Hubrich, M., and Spiess, H. W. (1998) Determination of end-to-end distances in a series of TEMPO diradicals of up to 2.8 nm length with a new four-pulse double electron electron resonance experiment. *Angew. Chem., Int. Ed. 37*, 2833−2837.
(16) Langen, R., Oh, K. J., Cascio, D., and Hubbell, W. L. (2000) Crystal structures of spin labeled T4 lysozyme mutants: implications for the interpretation of EPR spectra in terms of structure. *Biochemistry 39*, 8396−8405.
(17) Guo, Z., Cascio, D., Hideg, K., Kalai, T., and Hubbell, W. L. (2007) Structural determinants of nitroxide motion in spin-labeled proteins: tertiary contact and solvent-inaccessible sites in helix G of T4 lysozyme. *Protein Sci. 16*, 1069−1086.
(18) Guo, Z., Cascio, D., Hideg, K., and Hubbell, W. L. (2008) Structural determinants of nitroxide motion in spin-labeled proteins: solvent-exposed sites in helix B of T4 lysozyme. *Protein Sci. 17*, 228−239.
(19) Fleissner, M. R., Cascio, D., and Hubbell, W. L. (2009) Structural origin of weakly ordered nitroxide motion in spin-labeled proteins. *Protein Sci. 18*, 893−908.
(20) Kroncke, B. M., Horanyi, P. S., and Columbus, L. (2010) Structural origins of nitroxide side chain dynamics on membrane protein alpha-helical sites. *Biochemistry 49*, 10045−10060.
(21) Tombolato, F., Ferrarini, A., and Freed, J. H. (2006) Dynamics of the nitroxide side chain in spin-labeled proteins. *J. Phys. Chem. B 110*, 26248−26259.
(22) Sezer, D., Freed, J. H., and Roux, B. (2008) Parametrization, molecular dynamics simulation, and calculation of electron spin resonance spectra of a nitroxide spin label on a polyalanine alpha-helix. *J. Phys. Chem. B 112*, 5755−5767.
(23) Columbus, L., and Hubbell, W. L. (2004) Mapping backbone dynamics in solution with site-directed spin labeling: GCN4−58 bZip free and bound to DNA. *Biochemistry 43*, 7273−7287.
(24) Lovell, S. C., Word, J. M., Richardson, J. S., and Richardson, D. C. (2000) The penultimate rotamer library. *Proteins 40*, 389−408.
(25) Mchaourab, H. S., Lietzow, M. A., Hideg, K., and Hubbell, W. L. (1996) Motion of spin-labeled side chains in T4 lysozyme. Correlation with protein structure and dynamics. *Biochemistry 35*, 7692−7704.
(26) Lietzow, M. A., and Hubbell, W. L. (2004) Motion of spin label side chains in cellular retinol-binding protein: correlation with structure and nearest-neighbor interactions in an antiparallel beta-sheet. *Biochemistry 43*, 3137−3151.
(27) Freed, D. M., Khan, A. K., Horanyi, P. S., and Cafiso, D. S. (2011) Molecular origin of electron paramagnetic resonance line shapes on beta-barrel membrane proteins: The local solvation environment modulates spin-label configuration. *Biochemistry 50*, 8792−8803.
(28) Munoz, V., Thompson, P. A., Hofrichter, J., and Eaton, W. A. (1997) Folding dynamics and mechanism of beta-hairpin formation. *Nature 390*, 196−199.
(29) Bauer, M. C., Xue, W. F., and Linse, S. (2009) Protein GB1 folding and assembly from structural elements. *Int. J. Mol. Sci. 10*, 1552−1566.
(30) Morrone, A., Giri, R., Toofanny, R. D., Travaglini-Allocatelli, C., Brunori, M., Daggett, V., and Gianni, S. (2011) GB1 is not a two-state folder: identification and characterization of an on-pathway intermediate. *Biophys. J. 101*, 2053−2060.
(31) Thoms, S., Max, K. E., Wunderlich, M., Jacso, T., Lilie, H., Reif, B., Heinemann, U., and Schmid, F. X. (2009) Dimer formation of a stabilized Gbeta1 variant: a structural and energetic analysis. *J. Mol. Biol. 391*, 918−932.
(32) Nadaud, P. S., Helmus, J. J., Kall, S. L., and Jaroniec, C. P. (2009) Paramagnetic ions enable tuning of nuclear relaxation rates and provide long-range structural restraints in solid-state NMR of proteins. *J. Am. Chem. Soc. 131*, 8108−8120.
(33) Walsh, J. D., Meier, K., Ishima, R., and Gronenborn, A. M. (2010) NMR studies on domain diffusion and alignment in modular GB1 repeats. *Biophys. J. 99*, 2636−2646.
(34) Sengupta, I., Nadaud, P. S., Helmus, J. J., Schwieters, C. D., and Jaroniec, C. P. (2012) Protein fold determined by paramagnetic magic-angle spinning solid-state NMR spectroscopy. *Nature Chem. 4*, 410−417.
(35) Gronenborn, A. M., Filpula, D. R., Essig, N. Z., Achari, A., Whitlow, M., Wingfield, P. T., and Clore, G. M. (1991) A novel, highly stable fold of the immunoglobulin binding domain of streptococcal protein G. *Science 253*, 657−661.
(36) Alexander, P., Fahnestock, S., Lee, T., Orban, J., and Bryan, P. (1992) Thermodynamic analysis of the folding of the streptococcal protein G IgG-binding domains B1 and B2: why small proteins tend to have high denaturation temperatures. *Biochemistry 31*, 3597−3603.
(37) Lian, L. Y., Yang, J. C., Derrick, J. P., Sutcliffe, M. J., Roberts, G. C., Murphy, J. P., Goward, C. R., and Atkinson, T. (1991) Sequential 1H NMR assignments and secondary structure of an IgG-binding domain from protein G. *Biochemistry 30*, 5335−5340.
(38) Gallagher, T., Alexander, P., Bryan, P., and Gilliland, G. L. (1994) Two crystal structures of the B1 immunoglobulin-binding domain of streptococcal protein G and comparison with NMR. *Biochemistry 33*, 4721−4729.
(39) Franks, W. T., Wylie, B. J., Stellfox, S. A., and Rienstra, C. M. (2006) Backbone conformational constraints in a microcrystalline U-15N-labeled protein by 3D dipolar-shift solid-state NMR spectroscopy. *J. Am. Chem. Soc. 128*, 3154−3155.
(40) Wylie, B. J., Sperling, L. J., Nieuwkoop, A. J., Franks, W. T., Oldfield, E., and Rienstra, C. M. (2011) Ultrahigh resolution protein structures using NMR chemical shift tensors. *Proc. Natl. Acad. Sci. U.S.A. 108*, 16974−16979.
(41) (1994) The CCP4 suite: programs for protein crystallography. *Acta Crystallogr., Sect. D 50*, 760−763.
(42) McCoy, A. J., Grosse-Kunstleve, R. W., Adams, P. D., Winn, M. D., Storoni, L. C., and Read, R. J. (2007) Phaser crystallographic software. *J. Appl. Crystallogr. 40*, 658−674.

(43) Frericks Schmidt, H. L., Sperling, L. J., Gao, Y. G., Wylie, B. J., Boettcher, J. M., Wilson, S. R., and Rienstra, C. M. (2007) Crystal polymorphism of protein GB1 examined by solid-state NMR spectroscopy and X-ray diffraction. *J. Phys. Chem. B 111*, 14362−14369.
(44) Murshudov, G. N., Vagin, A. A., and Dodson, E. J. (1997) Refinement of macromolecular structures by the maximum-likelihood method. *Acta Crystallogr. Sect., D 53*, 240−255.
(45) Emsley, P., and Cowtan, K. (2004) Coot: model-building tools for molecular graphics. *Acta Crystallogr. Sect., D 60*, 2126−2132.
(46) Langer, G., Cohen, S. X., Lamzin, V. S., and Perrakis, A. (2008) Automated macromolecular model building for X-ray crystallography using ARP/wARP version 7. *Nat. Protocols 3*, 1171−1179.
(47) Zielke, V., Eickmeier, H., Hideg, K., Reuter, H., and Steinhoff, H.-J. (2008) A commonly used spin label: S-(2,2,5,5-tetramethyl-1-oxyl-[delta]3-pyrrolin-3-ylmethyl) methanethiosulfonate. *Acta Crystallogr., Sect. C 64*, o586−o589.
(48) Chen, V. B., Arendall, W. B., III, Headd, J. J., Keedy, D. A., Immormino, R. M., Kapral, G. J., Murray, L. W., Richardson, J. S., and Richardson, D. C. (2010) MolProbity: all-atom structure validation for macromolecular crystallography. *Acta Crystallogr. Sect., D 66*, 12−21.
(49) Stoll, S., and Schweiger, A. (2006) EasySpin, a comprehensive software package for spectral simulation and analysis in EPR. *J. Magn. Reson. 178*, 42−55.
(50) Budil, D. E., Lee, S., Saxena, S., and Freed, J. H. (1996) Nonlinear-least-squares analysis of slow-motion EPR spectra in one and two dimensions using a modified Levenberg−Marquardt algorithm. *J. Magn. Reson., Ser. A 120*, 155−189.
(51) Jeschke, G., Chechik, V., Ionita, P., Godt, A., Zimmermann, H., Banham, J., Timmel, C. R., Hilger, D., and Jung, H. (2006) DeerAnalysis2006 − a comprehensive software package for analyzing pulsed ELDOR data. *Appl. Magn. Reson.*, 473−498.
(52) Louis, J. M., Byeon, I. J., Baxa, U., and Gronenborn, A. M. (2005) The GB1 amyloid fibril: recruitment of the peripheral beta-strands of the domain swapped dimer into the polymeric interface. *J. Mol. Biol. 348*, 687−698.
(53) Jee, J., Byeon, I. J., Louis, J. M., and Gronenborn, A. M. (2008) The point mutation A34F causes dimerization of GB1. *Proteins 71*, 1420−1431.
(54) Kuhlman, B., O'Neill, J. W., Kim, D. E., Zhang, K. Y., and Baker, D. (2001) Conversion of monomeric protein L to an obligate dimer by computational protein design. *Proc. Natl. Acad. Sci. U.S.A. 98*, 10687−10691.
(55) O'Neill, J. W., Kim, D. E., Johnsen, K., Baker, D., and Zhang, K. Y. (2001) Single-site mutations induce 3D domain swapping in the B1 domain of protein L from *Peptostreptococcus magnus*. *Structure 9*, 1017−1027.
(56) Bode, B. E., Margraf, D., Plackmeyer, J., Durner, G., Prisner, T. F., and Schiemann, O. (2007) Counting the monomers in nanometer-sized oligomers by pulsed electron-electron double resonance. *J. Am. Chem. Soc. 129*, 6736−6745.
(57) Polyhach, Y., and Jeschke, G. (2010) Prediction of favourable sites for spin labelling of proteins. *Spectroscopy 24*, 651−659.
(58) Sarver, J. L., Townsend, J. E., Rajapakse, G., Jen-Jacobson, L., and Saxena, S. (2012) Simulating the dynamics and orientations of spin-labeled side chains in a protein-DNA complex. *J. Phys. Chem. B 116*, 4024−4033.